PAR protein activation-deactivation cycles stabilize long-axis polarization in *C. elegans*

Raphaela Geßele, Jacob Halatek, and Erwin Frey*
Arnold Sommerfeld Center for Theoretical Physics (ASC) and Center for NanoScience (CeNS), Department of Physics, Ludwig-Maximilians-Universität München, Theresienstrasse 37, 80333 München, Germany and Nanosystems Initiative Munich (NIM), Ludwig-Maximilians-Universität München, Schellingstraße 4, 80333 Munich, Germany
(Dated: October 24, 2018)

Cell polarity endows cells with a reference frame that guides cellular organization and division. In the *Caenorhabditis elegans* zygote, PAR protein patterns determine the anterior-posterior axis and facilitate the redistribution of proteins for the first asymmetric cell division. While previous theoretical work has shown that mutual antagonism between (anterior) aPAR and (posterior) pPAR proteins is the key to polarity maintenance, what factors determine the selection of the polarity axis remains unclear. Here we formulate a reaction-diffusion model in a realistic cell geometry, based on bimolecular reactions and fully accounting for the coupling between membrane and cytosolic dynamics. We find that the kinetics of the phosphorylation-dephosphorylation cycle of PAR proteins is crucial for the selection of the long (anterior-posterior) axis for polarization. Biochemical cycles based on mutual exclusion alone, without a delay in dephosphorylation, would lead to short (dorsal-ventral) axis polarization. Our analysis shows that the local ratio of membrane surface to cytosolic bulk volume is the main geometric cue to which patterns adapt, and the decisive parameter that determines axis selection is given by the ratio of the diffusive length of the phosphorylated (inactive) phase to the cell length. We quantify the effect of relative protein numbers and find that they primarily affect the robustness of protein pattern formation. In particular, robustness to variations in the phosphorylation rates increases if scaffold proteins like PAR-3 are more abundant than PKC-3, which phosphorylates pPARs. Together, our theoretical study reveals the crucial role of geometry in self-organized protein pattern formation: axis selection is based on the generic dependence of intracellular pattern-forming processes on the local ratio of membrane surface to cytosolic volume.

Cell polarization is a crucial process in development [1]. Well studied examples include localization of bud sites in *Saccharomyces cerevisiae* [2], apico-basal asymmetry in mammalian epithelial cells [3], and the asymmetric placement of the first cell division in *Caenorhabditis elegans* zygote [4]. A key question in such systems is how the correct polarity axis is established and robustly maintained.

In *C. elegans*, the anterior-posterior axis of the embryo is determined in the fertilized egg by a polarized distribution of PAR (partitioning defective) proteins [4–6]. Immediately before the establishment of polarization begins, the future anterior PARs (aPARs) cover the cell cortex uniformly, while posterior PARs (pPARs) are cytoplasmic [7]. After fertilization, contraction of the actomyosin network leads to cortical flows that displace cortical aPARs anteriorly, allowing cytoplasmic pPARs to bind in the posterior zone [8, 9]; see Fig. 1*A* [10]. Once these two PAR domains have formed (during the 'establishment phase') and have thereby established the anterior-posterior axis, they persist for several minutes through the 'maintenance' phase until cell division [5, 7].

Several independent *in vivo* experiments on *C. elegans* have demonstrated that maintenance of PAR protein polarity is independent of an intact actomyosin network [7, 11–14]. Rather, it appears that the entry of the sperm and the following contractions of the cortical actomyosin serve as a temporal trigger for the establishment of the PAR protein pattern [9, 12, 15]. How then is formation of the pattern biochemically established and how is it stably maintained? Based on the fact that aPAR and pPAR proteins mutually drive each other off the membrane by phosphorylation [16], and that this antagonism promotes formation of distinct domains on the membrane [17–19], previous studies have outlined how self-organization of PAR proteins maintain polarization until cell division [14, 15]. These studies showed that basic features of PAR protein polarization can be explained by minimal reaction-diffusion models. However, as these models used a simplified one-dimensional geometry and assumed that cytosolic proteins are homogeneously distributed, the effect of cell geometry was disregarded and the distinction between long and short axis was lost. Thus, how the long axis is selected for polarization and subsequently maintained, and in a broader context, which features of a reaction-diffusion system are responsible for axis selection remain open questions.

To answer these questions we draw on previous studies of other intracellular pattern-forming protein systems which revealed that even the typically rather fast cytosolic diffusion does not eliminate protein gradients in the cytosol [20–23]. As a consequence, protein patterns are generically sensitive to cell geometry through coupling between processes in the cytosol and on the membrane. In particular, it was predicted [20, 21] that delayed reattachment to the cell membrane (e.g., due to cytosolic nucleotide exchange) is key to geometry sensing. Indeed,

* frey@lmu.de

recent experimental studies support the idea that axis selection depends on the interplay between reaction kinetics and cellular geometry [22].

These results suggest that the protein dynamics in the cytoplasm of the *C. elegans* embryo may also influence the selection of the long over the short axis during polarity maintenance. In order to investigate axis alignment, we developed a reaction-diffusion model of the PAR protein dynamics in the fertilized egg. As in previous studies [9, 14, 24], a central element in our model is mutual displacement of membrane-bound aPARs and pPARs by phosphorylation. However, in contrast to earlier models [9, 25], we do not use effective nonlinearities but strictly biomolecular reactions based on mass-action law kinetics, e.g. by explicitly modeling the formation of PAR protein complexes. Importantly, we also account for the delay caused by the need for reactivation of detached PAR proteins by cytosolic dephosphorylation, thus introducing the generic feature of a biochemical activation-deactivation cycle. As we will show, this feature is of particular relevance in a realistic cell geometry where diffusion and reactions of proteins on the membrane and in the cytosol are fully accounted for.

Our extended reaction-diffusion model in realistic cell geometry reveals that the dynamics of the phosphorylation-dephosphorylation cycle of PAR proteins is crucial for long-axis polarization. Without this additional feature, the biochemical network of PAR proteins would lead to the selection of short- instead of long-axis polarity in the single-cell embryo. Furthermore, we characterize the roles of mutual antagonism (phosphorylation) and overall protein numbers in robust long-axis polarization: while the phosphorylation rates determine how distinctively one polarization axis is selected over the other, relative protein numbers primarily affect the robustness of pattern formation as a whole.

Most importantly, our analysis indicates that these findings can be generalized beyond the specific model for the PAR system: axis selection is based on the generic dependence of intracellular pattern forming processes on the local ratio of membrane surface to cytosolic volume. Broadly speaking, this ratio determines the likelihood that a given protein will reattach to the membrane after detachment into the cytosol.

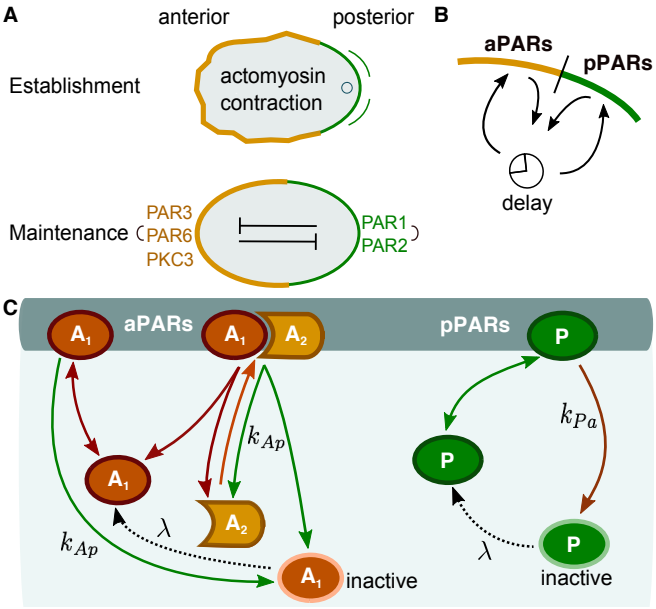

FIG. 1. (*A*) Cell polarization in the *C. elegans* embryo during the establishment (top) and maintenance (bottom) phases; sketch adapted from Ref. [5]. (*B*) Illustration of the protein flux between cytosol and membrane. As proteins detach from the membrane when phosphorylated, they cannot immediately rebind to the membrane. There is therefore an intrinsic delay before dephosphorylation permits rebinding. (*C*) The biochemical reaction network is comprised of two mutually antagonistic sets of proteins, aPARs and pPARs. Dephosphorylated (active) A_1 and P attach to the membrane with rates $k_{\mathrm{a}}^{\mathrm{on}}$ and $k_{\mathrm{p}}^{\mathrm{on}}$, respectively. Both active proteins may also detach spontaneously from the membrane with rates $k_{\mathrm{a}}^{\mathrm{off}}$ and $k_{\mathrm{p}}^{\mathrm{off}}$, respectively. A_1 acts as a scaffold protein: Once bound to the membrane it recruits A_2 with rate k_{d} and forms a membrane-bound heterodimeric aPAR complex A_{12}. The heterodimer A_{12} may itself spontaneously detach from the membrane with rate $k_{\mathrm{a}}^{\mathrm{off}}$ and dissociate into A_2 and active A_1. Membrane-bound A_1 and A_{12} can also be phosphorylated by P with rate $k_{\mathrm{Ap}}[P]$, thereby initiating dissociation of the aPAR complex and release of the aPAR proteins into the cytosol. While reattachment of the scaffold protein A_1 is delayed by the requirement for dephosphorylation (reactivation), detached A_2 can be recruited to the membrane by membrane-bound A_1 immediately. Similarly, P is phosphorylated by the heterodimer A_{12} at rate $k_{\mathrm{Pa}}[A_{12}]$, and is consequently released as inactive P into the cytosol. In the same way as A_1, also P must be dephosphorylated before it can bind again to the membrane. For simplicity, we take identical dephosphorylation (reactivation) rates λ for inactive A_1 and P. The ensuing reaction-diffusion equations and a table listing the values of the rate constants are provided in the SI section **S.I.**.

REACTION-DIFFUSION MODEL

The aPAR set of proteins comprises PAR-3, PAR-6, and the atypical protein kinase PKC-3. Only complexes containing PKC-3 can phosphorylate pPARs, thereby disabling their membrane-binding capacity [17, 26]. How trimeric complexes consisting of PAR-3, PAR-6 and PKC-3 actually form is not fully understood. The evidence so far suggests that PAR-6 acts as a linker between PKC-3 and PAR-3, which can itself bind directly to the membrane [27–30]. In the absence of PAR-6, PKC-3 freely diffuses in the cytosol [31, 32]. In the reaction network upon which our mathematical model is based, we simplify the formation of trimeric complexes to the formation of a complex consisting of two effective species of aPARs: A_1 and A_2 (Fig. 1*C*). The first species, A_1, models the membrane binding function of PAR-3, thus we also refer to it as a scaffold protein. The second species,

A_2, corresponds to a complex of PAR-6 and PKC-3. It is assumed to be recruited by scaffold proteins A_1 that are already bound to the membrane, thereby forming hetero-dimers A_{12} on the membrane which correspond to trimeric complexes. These complexes can then phosphorylate membrane-bound pPARs, which initiates their release into the cytosol in a phosphorylated (inactive) state.

As with aPARs, there are different pPAR species, PAR-1 and PAR-2. While it is known that PAR-2 binds directly to the membrane, and PAR-1 phosphorylates PAR-3, it remains unclear whether PAR-2 also helps to maintain anterior-posterior polarity by excluding aPAR complexes from the membrane [7, 16]. However, PAR-2 is required for posterior binding of PAR-1 [33] and PAR-2 exclusion from the membrane by PKC-3 is essential for proper restriction of pPARs to the posterior [17]. In view of the remaining uncertainties, and for the sake of simplicity, we refrain from distinguishing between different species and effectively treat the pPARs as a single species P (Fig. 1*C*). P phosphorylates membrane-bound A_1 and A_{12}, which triggers their subsequent detachment as a phosphorylated (inactive) species into the cytosol.

To provide a realistic cell geometry (prolate spheroid) similar to that previously employed in studies of Min oscillations in *E. coli* [20], we use a two-dimensional elliptical geometry with long axis $a \approx 27\,\mu m$ and short axis $b \approx 15\,\mu m$. The boundary and interior of the ellipse represent the cell membrane and cytosolic volume, respectively. In addition to cytosolic diffusion, our model also accounts for protein dephosphorylation reactions in the cytosol. This creates deactivation-reactivation cycles, as proteins that were phosphorylated (deactivated) on the membrane are thereby reactivated for membrane binding (Fig. 1*B*, *C*). For simplicity, the reactivation (dephosphorylation) rate λ is assumed to be identical for cytosolic pPARs (P) and aPARs (only A_1). The ensuing reaction-diffusion equations are given in section **S.I.** of the Supplementary Material.

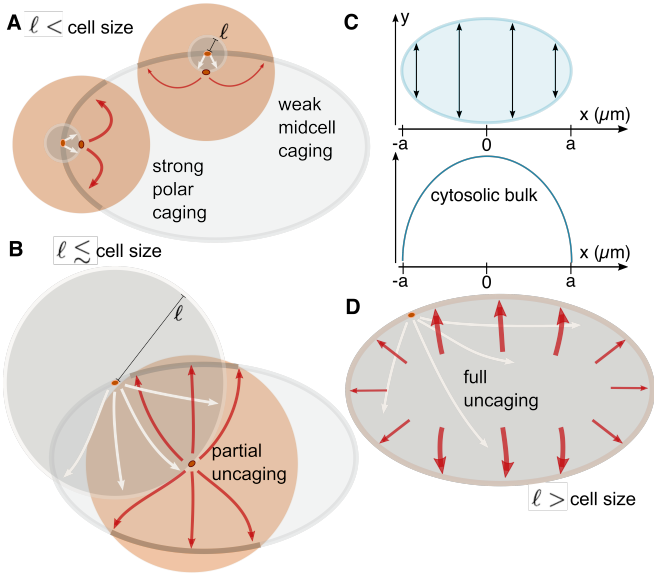

FIG. 2. **Role of dephosphorylation in axis determination.** (*A*) If the reactivation length ℓ is small compared to the cell size, the local membrane surface to cytosolic volume ratio strongly affects the position at which detached proteins reattach. A protein that detaches from a cell pole is more likely to reattach near that same cell pole than a protein detaching from midcell is to reattach at midcell. Hence, dynamics that are based on membrane-cytosol cycling (such as antagonistic reactions that maintain an interface) are enhanced at the cell poles. (*B*) As the reactivation length ℓ approaches the length of the cell, this effect of geometry becomes weaker, and detaching proteins become increasingly unconstrained by the position of detachment (*uncaged*). (*C*) Illustration of the distribution of cytosolic bulk proteins along the long axis. (*D*) This effect of cell geometry is completely lost if the reactivation length ℓ exceeds the length of the cell. Hence, detached proteins become uniformly distributed throughout the cell before reactivation occurs. In that case, most will re-encounter the membrane near midcell after reactivation, since a delocalized protein will most likely be found in the midcell area.

RESULTS

Cytosolic dephosphorylation plays a key role for axis determination

For mutually antagonistic protein interactions as in the PAR system, protein domains are separated by an interface at which mutually induced membrane detachment dominates [9, 14, 15]. For this interface (and the protein domains it separates) to be maintained, proteins that have detached from the membrane must be replaced, otherwise the antagonistic interaction between the proteins would deplete either aPARs or pPARs from the membrane. As the protein interactions are mass-conserving, maintenance requires that detached proteins quickly rebind, unless the cytosolic reservoir of proteins is large enough for them to be replenished directly. This suggests that an interface can best be maintained in those membrane regions where rebinding to the membrane after detachment is most likely.

The likelihood of rebinding is in turn determined by the availability of cytosolic proteins for binding, which is a function of the interplay of two factors: the local cell geometry and the time required for reactivation of the detached proteins by dephosphorylation (Fig. 2). Due to different local membrane curvatures in a cell, the ratio of available membrane surface to cytosolic volume is highest at cell poles and lowest at midcell. How the local cell geometry affects protein rebinding depends on the dephosphorylation time: a longer reactivation time implies that a protein that detached in a phosphorylated state from the membrane will on average diffuse farther away from the membrane before it can be reactivated and reattaches. As in a standard diffusion-degradation problem [34], the corresponding *reactivation length* is es-

timated as $\ell := \sqrt{D_{\rm cyt}/\lambda}$.

To see how this diffusion length affects protein dynamics, consider a protein with a short inactive (phosphorylated) phase, such that ℓ is significantly smaller than the cell size $L = 2a$ (Fig. 2*A*). Then, proteins are likely to be dephosphorylated fast and can therefore rebind very soon after phosphorylation-induced detachment. Since the local ratio of membrane surface to cytosolic volume at the cell poles is larger than at midcell, these proteins are more likely to reencounter the membrane in the polar zone which translates into higher polar reattachment (after reactivation), i.e. proteins remain *caged* at the cell poles (Fig. 2*A*). Conversely, proteins that detached from the membrane at midcell have more cytosolic volume available than those that detached at the poles and, thus, are less likely to re-encounter the membrane and rebind there (Fig. 2*A*). This heuristic picture suggests that for $\ell \ll L$ domain interfaces preferentially form at the cell poles and hence cell polarity will be established along the short axis.

If dephosphorylation requires more time, ℓ increases and the effect of local membrane curvature (ratio of membrane surface to cytosolic volume) is attenuated (Fig. 2*B*). As the reactivation length approaches the cell size ($\ell \lesssim L$), the farther detached proteins can diffuse from their detachment position. Ultimately, when $\ell > L$, proteins can be considered as uniformly distributed throughout the cytosol for the next attachment event (Fig. 2*D*). Therefore, reactivated proteins are more likely to attach at midcell, where the accumulated density along the long axis (or, equivalently, the ratio of cytosolic volume to membrane area) is highest (Fig. 2*C*). This implies that an interface between different protein domains will establish itself at midcell and cells will become polarized along the long axis for large enough reactivation length ℓ.

In summary, if cell polarization is induced by antagonistic protein interaction as in *C. elegans*, we expect long axis polarization only if the delay resulting from the inactive phase is sufficiently long. Moreover, our heuristic analysis also suggests that relative protein numbers affect axis selection, as the global availability of an abundant protein species attenuates effect of cell geometry associated with the activation-deactivation cycle.

Linear stability analysis

To put the above heuristic reasoning on a firm basis and gain a deeper understanding of the mechanisms underlying axis selection, we performed a mathematical analysis, building on previous investigations of intracellular pattern formation in elliptical cell geometry [20, 21].

Importantly, in the bounded geometry of a cell, broken detailed balance due to the dephosphorylation-phosphorylation cycle – more generally an activation-deactivation cycle – implies that a uniform well-mixed state can no longer be a steady state of the system [21].

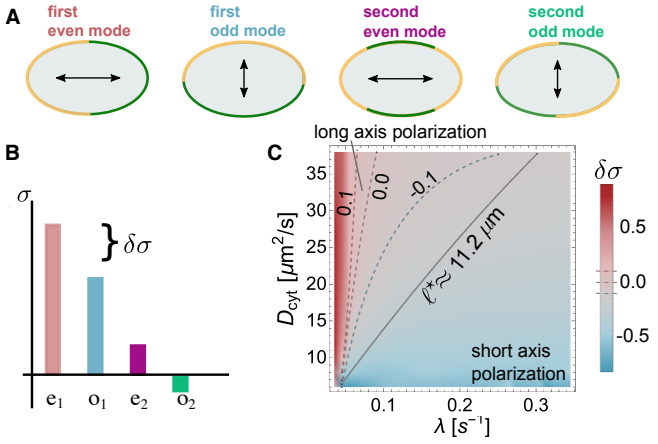

FIG. 3. **Mode selection and the polarity axis.** (*A*) Illustration of the protein distribution on the membrane and the ensuing polarity axis for the lowest-order even and odd modes. (*B*) Illustration of the mode spectrum for these lowest-order modes and the gap $\delta\sigma$ in the growth rates between the first even and first odd mode. (*C*) Relative difference in the growth rates of the first even and odd modes (linear stability analysis in color code), $\delta\sigma$, as a function of $D_{\rm cyt}$ and λ. For small λ and large $D_{\rm cyt}$, $\delta\sigma$ is clearly greater than zero (red, long axis polarization), whereas for large λ and small $D_{\rm cyt}$, $\delta\sigma$ lies below zero (blue, short axis polarization). These findings are validated using FEM simulations. FEM sweeps in $D_{\rm cyt}$ and λ were run until the steady state was reached. These simulations yielded a straight-line interface (black-solid line in (*C*)) in the λ-$D_{\rm cyt}$ parameter space which divides long (above) from short (below) axis polarization in steady state. The line corresponds to a constant threshold reactivation length $\ell^\star$. All parameters other than $D_{\rm cyt}$ and λ can be found in **TABLE S.I.** in the SI.

Instead, all steady states show cytosolic gradients with a density profile that is spatially non-uniform but unpolarized [21]. These near-uniform steady states can be well approximated by states with a homogeneous protein concentrations on the membrane and a cytosolic protein gradient perpendicular to the membrane [20]; see also section **S.II.** in the Supplementary Information. As the reactive dynamics in the PAR system is bistable, there are two such unpolarized states, one with aPAR and the other with pPAR being the more abundant membrane species. In the zygote, aPARs predominate on the membrane, and we refer to this aPAR-dominant state as the *unpolarized state*.

To perform a linear stability analysis with respect to this unpolarized state, we use Fourier modes specific for the elliptical cell geometry [20]. These modes are classified as even and odd by their symmetry with respect to reflections through a plane along the long axis, and correspond to membrane patterns aligned along the long and short axes, respectively (Fig. 3*A*). If the real parts of the growth rates σ of all Fourier modes are negative, small spatial perturbations of the unpolarized state will decay and it will remain stable. In contrast, a positive real part of any growth rate indicates that the unpolarized

state is unstable to spatial perturbations, and initially a pattern will emerge corresponding to the mode with the highest growth rate (Fig. 3*B*). Hence, linear stability analysis informs about the parameter regime where patterns of a certain symmetry (short vs. long axis) form spontaneously. We expect that these pattern attractors persist for some range outside the linear unstable parameter regime (see section **S.III.** in the SI), where patterns do not form spontaneously but can be triggered by a finite perturbation — such as the fertilization event.

For a typical cell size and cytosolic diffusion constants in the range of 5–50 $\mu m^2/s$, our linear stability analysis shows that second- and higher-order modes are negligible compared to the first even and odd modes, σ_e and σ_o, respectively. In the parameter regime under consideration, those two growth rates exhibit similar magnitude and at least one of them is positive. To quantify the competition between the first even and odd modes (long vs. short axis), we define the relative difference in their growth rates, $\delta\sigma := (\sigma_e - \sigma_o)/\sqrt{\sigma_e^2 + \sigma_o^2}$; for an illustration see Fig. 3*B*.

Cytosolic reactivation length determines the polarization axis

We computed $\delta\sigma$ as a function of λ and D_{cyt}. As shown in Fig. 3*C*, the even mode dominates ($\delta\sigma > 0$) for $\ell \gtrsim 15\,\mu m$; otherwise the odd mode dominates. This is consistent with the above heuristic reasoning suggesting that reactivation must be slow or cytosolic diffusion must be fast for long-axis polarity. To test whether the linear stability analysis correctly predicts the final polarization axis, we performed finite-element (FEM) simulations; see also section **S.III.** in the SI. These simulations show that there is a threshold value for the reactivation length $\ell^\star = 11.2\ \mu m$ (approximately 20% of the cell length L) above/below which cells stably polarize along the long/short axis (Fig. 3*C*). We conclude that the reactivation length ℓ, which determines the spatial distribution of active proteins, is the decisive parameter that determines axis selection.

Relative phosphorylation rates restrict the spontaneous emergence of polarization

Whether there is a spatial separation between aPAR and pPAR domains, is known to depend on the relative magnitude of the phosphorylation rates k_{Ap} and k_{Pa} [9, 15]: an interface between different domains exists and can be maintained only if these antagonistic phosphorylation processes are balanced. To determine the necessary conditions for this balance, we analyzed the stability of the unpolarized state numerically, while varying both phosphorylation rates over one order of magnitude. The cytosolic diffusion constant was kept fixed at $D_{cyt} = 30\,\mu m^2/s$, and we chose two representative reactivation rates, $\lambda = 0.3\,s^{-1}$ and $\lambda = 0.05\,s^{-1}$, corresponding to reactivation lengths, $\ell = 10\,\mu m$ and $\ell = 24.5\,\mu m$, respectively.

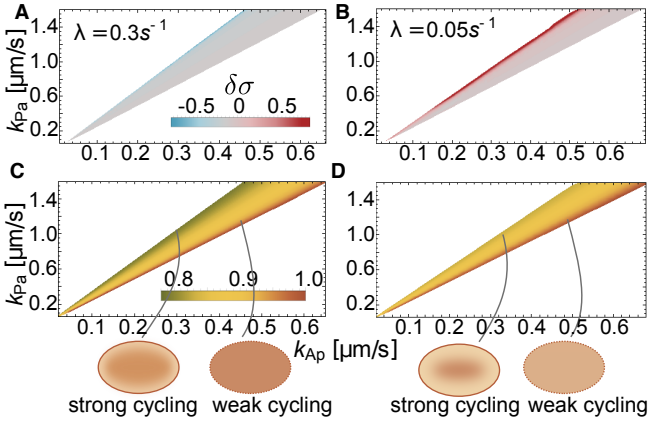

FIG. 4. **Role of phosphorylation rates for polarization and axis selection.** Linear stability analysis shows that spontaneous polarization is possible only within a range of ratios between the phosphorylation rates, k_{Pa}/k_{Ap} (cone-shaped regions): The relative difference in the growth rates of even and odd modes ($\delta\sigma$) is shown in (*A*) for $\lambda = 0.3\,s^{-1}$, and (*B*) for $\lambda = 0.05\,s^{-1}$ in color code (indicated in the graph). Panels (*C*) and (*D*) show the corresponding cytosolic concentration of A_1 in the aPAR dominant unpolarized state (A_2 has a quantitatively similar concentration gradient to A_1 within the cone, not shown), normalized with respect to the maximal concentration of A_1 obtained within the respective cone. Cartoons at the bottom of the figure schematically depict the cytosolic distribution of aPARs throughout the cell.

Our analysis in full cell geometry shows that spontaneous polarization starting from the unpolarized state arises only within a limited range of k_{Pa}/k_{Ap} values (cones in Fig. 4), in accordance with previous theoretical studies using a simplified one-dimensional model [9, 25]. Strikingly, our results also show that the selection of the polarization axis does not depend on the nonlinear processes (mutual antagonism) but primarily on the linear activation-deactivation cycle, i.e. the relative magnitude of reactivation length and cell size, ℓ/L. The ratio of the phosphorylation rates mainly determines the initial preference for a polarization axis starting from an unpolarized state (Fig. 4*A*, *B*).

Specifically, we find that for $\lambda = 0.3\,s^{-1}$, the first even mode grows more slowly than the first odd mode ($\delta\sigma < 0$), favoring short-axis polarization. The results are more diverse for $\lambda = 0.05\ s^{-1}$. Here, for large k_{Pa}/k_{Ap}, the first even mode grows faster than the first odd mode ($\delta\sigma > 0$). In contrast, for the mid to low range of k_{Pa}/k_{Ap}, one finds $\delta\sigma \approx 0$, i.e. linear stability analysis does not predict a clear preference for either long- or short-axis polarization. FEM simulations show, however, that – irrespective of the ratio k_{Pa}/k_{Ap} – long- and short-axis polarization in the final steady state is obtained for $\ell = 10\,\mu m$ and $\ell = 24.5\,\mu m$, respectively; see **S.III.** in the SI. These simulations confirm that the reactivation length ℓ is the de-

ciding factor in for axis selection. The FEM simulations further show that outside of the parameter regime of linear instability there exist stable polarized states, showing that the system is *excitable*, i.e. that patterns can be triggered by a finite perturbation; see section **S.III.** in the SI.

The dependence of the initial growth rates on the ratio of phosphorylation rates can be attributed to the fact that, in the unpolarized (aPAR-dominant state), the cytosolic concentration of aPARs increases with the rate at which aPARs are phosphorylated by pPARs, i.e. with a reduction in the ratio $k_{\mathrm{Pa}}/k_{\mathrm{Ap}}$ (Fig. 4*C*, *D*). If a protein species is abundant in the cytosol, recycling of recently detached proteins can be compensated for by a protein of the same type in the cytosolic reservoir attaching to the membrane. Hence, geometry effects in the initial polarization phase are expected to dominate if the cytosolic pool of proteins undergoing an activation-deactivation cycle is low, explaining why $\delta\sigma$ depends on geometry for large values of $k_{\mathrm{Pa}}/k_{\mathrm{Ap}}$.

Robustness of polarization as well as axis selection depend on the relative protein densities

After learning that the abundance of cytosolic proteins determines initial axis selection, we asked how changing the relative *total* protein densities affects cell polarization. A linear stability analysis revealed that density variations alter several features: the range of ratios $k_{\mathrm{Pa}}/k_{\mathrm{Ap}}$ for which an interface between different PAR domains can be stably maintained, and the threshold value of reactivation length $\ell^\star$ that distinguishes between short- and long-axis polarization. The effects were most prominent when the ratio of pPAR and aPAR proteins that phosphorylate each other ($[P]/[A_2]$), and the ratio of aPAR proteins ($[A_1]/[A_2]$) was varied.

As shown in Fig. 5, varying the ratio of the antagonistic proteins ($[P]/[A_2]$) mainly shifts the regime of spontaneous cell polarization up on the $k_{\mathrm{Pa}}/k_{\mathrm{Ap}}$ axis. This shift is easily explained, as the effective mutual phosphorylation rates are given by $k_{Ap}[P]$ and $k_{Pa}[A_{12}]$, respectively – where $[A_{12}]$ is mainly limited by the availability of $[A_2]$. Therefore, when the concentration of pPAR proteins ($[P]$) is increased relative to $[A_2]$, the per capita rate k_{Pa} has to be increased relative to k_{Ap} as well, in order to retain the balance between the mutual phosphorylation processes.

Changing the ratio between the different types of aPAR proteins has two effects. First, spontaneous polarization is possible for a broader range of $k_{\mathrm{Pa}}/k_{\mathrm{Ap}}$. Increasing the concentration of the scaffold protein $[A_1]$ relative to $[A_2]$, which phosphorylates pPARs, decreases the lower bound of $k_{\mathrm{Pa}}/k_{\mathrm{Ap}}$ that allows for polarization. This is a consequence of the increased reservoir size of A_1 which implies a higher rate of attachment of cytosolic A_1 to the membrane and hence a fast local redimerization of A_2 (which lacks an inactive phase) right after the detachment of a heterodimer A_{12}. This newly formed heterodimer A_{12} is then competent to phosphorylate pPARs. Thus it is plausible that even for low $k_{\mathrm{Pa}}/k_{\mathrm{Ap}}$ one can achieve a balance of mutual antagonism, extending the lower bound of the polarization regime. Second, changing the ratio $[A_1]/[A_2]$ also has a major effect on the threshold value of the reactivation length $\ell^\star$. We find that $\ell^\star$ increases with increasing concentration of the scaffold protein $[A_1]$ (Fig. 5). Again, this can be understood as a reservoir effect: globally abundant A_1 promotes immediate re-dimerization of A_2 with any available A_1. Axis selection is then affected by the *polar recycling* of A_2.

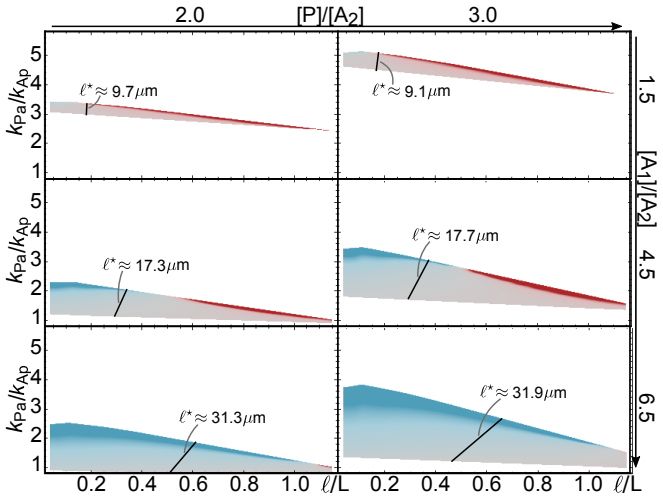

FIG. 5. **Relative protein numbers determine the robustness of cell polarity.** Linear stability analysis for a range of density ratios $[P]/[A_2]$ and $[A_1]/[A_2]$ indicated in the graph; $[A_2]$ was kept constant. Each graph shows the range of phosphorylation ratios ($k_{\mathrm{Pa}}/k_{\mathrm{Ap}}$) and relative reactivation lengths (ℓ/L) where the *base state* is linearly unstable, with $\delta\sigma$ given by the same color code as in Fig. 4*A*; fixed parameters are $k_{\mathrm{Ap}} = 0.4\,\mu m/s$ and $D_{\mathrm{cyt}} = 30\,\mu m^2/s$, and further parameters not varied can be found in **TABLE S.I.** of the SI. FEM parameter sweeps of k_{Pa} and λ, with fixed parameters $k_{\mathrm{Ap}} = 0.4\,\mu m/s$ and $D_{\mathrm{cyt}} = 30\,\mu m^2/s$, for each density set show that the steady state polarization axis also depends strongly on the ratio $[A_1]/[A_2]$. The steady state switches from short- to long-axis polarization at the black line in each graph, indicating $\ell^\star$.

Taken together, both of these findings emphasize the importance of the activation-deactivation cycle. A cell polarizes more robustly for higher amounts of *scaffold* proteins. However, at the same time, the cytosolic reactivation length has to increase significantly in order to also robustly maintain long-axis polarization.

DISCUSSION

Here, we have addressed two linked questions concerning cell polarity in *C. elegans*: Under what conditions do cells polarize, and what determines the polarization

axis?

Previous experiments supported by mathematical models in simplified cell geometry have indicated that a balance between mutual phosphorylation of aPAR and pPAR proteins is the key mechanism responsible for cell polarization [9, 14, 15, 35]. Our theoretical results in realistic cell geometry support this finding. In addition, we have shown here that the robustness of cell polarity to variations in the phosphorylation rates increases if the scaffold protein PAR-3 is more abundant than PKC-3, which phosphorylates pPARs. Hence, low scaffold abundance is incompatible with robust biological function. This agrees with experimental findings that the scaffold function of PAR-3 is at least partially supported by other proteins (e.g. Cdc-42 [30]). Our results suggest that it would be worthwhile to experimentally search for other scaffold proteins and test their functional roles in axis selection.

Most importantly, our theoretical analysis in realistic cell geometry reveals that the key feature of the biochemical network responsible for axis selection is the phosphorylation-dephosphorylation cycle of PAR-3 and PAR-2 that leads to a delayed rebinding after detachment from the membrane, and the absence of such a delay for rebinding of the complex of PKC-3 and PAR-6. The reactivation time (λ^{-1}) implies a cytosolic reactivation length $\ell = \sqrt{D_{\rm cyt}/\lambda}$ which defines a cytosolic zone of inactive proteins close to the membrane. As a consequence, proteins with a small reactivation length remain partially caged at the cell poles after membrane detachment, while those with a large reactivation length are uncaged and thereby become uniformly distributed in the cytosol before rebinding. Similarly, proteins lacking a delay, like PKC-3, are available for rebinding immediately after detachment from the membrane and are thus strongly caged to the cell poles. Our theoretical analysis shows that long axis polarization is stable only for sufficiently large ℓ. The threshold value for the reactivation length ℓ depends on the ratio of PAR-3 to PKC-3: a larger cytosolic pool of PAR-3 attenuates the effect of selecting the interface at midplane and at the same time strengthens the effect of PKC-3 to put the interface at the poles. Hence we predict that increasing the number of PAR-3 destabilizes long axis polarization in favor of short axis polarization.

On a broader perspective, these results show that selection of a characteristic wavelength for a pattern and selection of a polarity axis are distinct phenomena and are, in general, mediated by different underlying mechanisms (See **S.II**). We expect the following findings to be generic for mass-conserved intracellular protein systems: cells sense the cellular geometry by the local membrane to bulk ratio, an activation-deactivation cycle can act as a pattern axis switching mechanism, and cytosolic protein reservoirs alter the sensitivity to cell geometry. Identifying the biochemical steps that are most relevant for axis selection in other intracellular pattern forming systems is an important theme for future research.

ACKNOWLEDGMENTS

We would like to thank T. Fehm and T. Meinhardt who were involved at early, preliminary stages of this project, and F. Brauns, L. Hassan and B. Osberg for critical reading of the manuscript and for providing valuable feedback. E.F. acknowledges support from the German Excellence Initiative via the program 'NanoSystems Initiative Munich' (NIM) and the Deutsche Forschungsgemeinschaft (DFG) via project B02 within the Collaborative Research Center SFB 1032. R.G. is supported by a DFG fellowship through the Graduate School 'Quantitative Bioscience Munich' (QBM).

[1] J. P. Campanale, T. Y. Sun, and D. J. Montell, "Development and dynamics of cell polarity at a glance," *J Cell Sci*, vol. 130, no. 7, pp. 1201–1207, 2017.

[2] J.-g. Chiou, M. K. Balasubramanian, and D. J. Lew, "Cell polarity in yeast," *Annu Rev Cell Dev Biol*, vol. 15, pp. 365–391, 2017.

[3] J. Roignot, X. Peng, and K. Mostov, "Polarity in mammalian epithelial morphogenesis," *Cold Spring Harb Protoc*, vol. 33, 2013.

[4] N. W. Goehring, "PAR polarity: from complexity to design principles.," *Exp Cell Res*, vol. 328, no. 2, pp. 258–266, 2014.

[5] B. Goldstein and I. G. Macara, "The PAR proteins: fundamental players in animal cell polarization," *Dev Cell*, vol. 13, no. 5, pp. 609–622, 2007.

[6] P. Gönczy, "Asymmetric cell division and axis formation in the embryo," *WormBook*, pp. 1–20, 2005.

[7] A. A. Cuenca, A. Schetter, D. Aceto, K. Kemphues, and G. Seydoux, "Polarization of the C. elegans zygote proceeds via distinct establishment and maintenance phases," *Development*, vol. 130, no. 7, pp. 1255–1265, 2003.

[8] E. Munro, J. Nance, and J. R. Priess, "Cortical flows powered by asymmetrical contraction transport PAR proteins to establish and maintain anterior-posterior polarity in the early C. elegans embryo," *Dev Cell*, vol. 7, no. 3, pp. 413–424, 2004.

[9] N. W. Goehring, P. K. Trong, J. S. Bois, D. Chowdhury, E. M. Nicola, a. a. Hyman, and S. W. Grill, "Polarization of PAR proteins by advective triggering of a pattern-forming system," *Science*, vol. 334, no. 6059, pp. 1137–1141, 2011.

[10] F. Motegi and G. Seydoux, "The PAR network: redundancy and robustness in a symmetry-breaking system.," *Philos Trans R Soc Lond B Biol Sci*, vol. 368, no. 1629, p. 20130010, 2013.

[11] D. P. Hill and S. Strome, "An analysis of the role of microfilaments in the establishment and maintenance of asymmetry in Caenorhabditis elegans zygotes.," *Dev Biol*, vol. 125, no. 1, pp. 75–84, 1988.

[12] C. R. Cowan and A. A. Cowan, "Centrosomes direct cell polarity independently of microtubule assembly in C. elegans embryos," *Nature*, vol. 431, no. 7004, pp. 92–96, 2004.

[13] Z. Petrásek, C. Hoege, A. Mashaghi, T. Ohrt, A. a. Hyman, and P. Schwille, "Characterization of protein dynamics in asymmetric cell division by scanning fluorescence correlation spectroscopy.," *Biophys J*, vol. 95, no. 11, pp. 5476–5486, 2008.

[14] A. T. Dawes and E. M. Munro, "PAR-3 oligomerization may provide an actin-independent mechanism to maintain distinct par protein domains in the early Caenorhabditis elegans embryo," *Biophys J*, vol. 101, no. 6, pp. 1412–1422, 2011.

[15] N. W. Goehring, C. Hoege, S. W. Grill, and A. Hyman, "PAR proteins diffuse freely across the anterior-posterior boundary in polarized C. elegans embryos," *J Cell Biol*, vol. 193, no. 3, pp. 583–594, 2011.

[16] C. Hoege and A. A. Hyman, "Principles of PAR polarity in Caenorhabditis elegans embryos," *Nat Rev Mol Cell Biol*, vol. 14, no. 5, pp. 315–322, 2013.

[17] Y. Hao, L. Boyd, and G. Seydoux, "Stabilization of cell polarity by the c. elegans ring protein par-2," *Dev Cell*, vol. 10, no. 2, pp. 199–208, 2006.

[18] S. Zonies, F. Motegi, Y. Hao, and G. Seydoux, "Symmetry breaking and polarization of the C. elegans zygote by the polarity protein PAR-2.," *Development*, vol. 137, no. 10, pp. 1669–1677, 2010.

[19] F. Motegi, S. Zonies, Y. Hao, A. A. Cuenca, E. Griffin, and G. Seydoux, "Microtubules induce self-organization of polarized PAR domains in Caenorhabditis elegans zygotes.," *Nat Cell Biol*, vol. 13, no. 11, pp. 1361–7, 2011.

[20] J. Halatek and E. Frey, "Highly canalized MinD transfer and MinE sequestration explain the origin of robust MinCDE-protein dynamics," *Cell Rep*, vol. 1, no. 6, pp. 741–752, 2012.

[21] D. Thalmeier, J. Halatek, and E. Frey, "Geometry-induced protein pattern formation.," *Proc Natl Acad Sci USA*, vol. 113, no. 3, pp. 548–553, 2016.

[22] F. Wu, J. Halatek, M. Reiter, E. Kingma, and E. Frey, "Multistability and dynamic transitions of intracellular Min protein patterns," *Mol Syst Biol*, vol. 12, no. 6, p. 873, 2016.

[23] J. Halatek and E. Frey, "Rethinking pattern formation in reaction-diffusion systems," *Nat Phys*, vol. 14, no. 5, pp. 507–514, 2018.

[24] A. T. Dawes and D. Iron, "Cortical geometry may influence placement of interface between Par protein domains in early Caenorhabditis elegans embryos.," *J Theor Biol*, vol. 333, pp. 27–37, 2013.

[25] P. K. Trong, E. M. Nicola, N. W. Goehring, K. V. Kumar, and S. W. Grill, "Parameter-space topology of models for cell polarity," *New J Phys*, vol. 16, no. 6, p. 65009, 2014.

[26] Y. Tabuse, Y. Izumi, F. Piano, K. J. Kemphues, J. Miwa, and S. Ohno, "Atypical protein kinase C cooperates with PAR-3 to establish embryonic polarity in Caenorhabditis elegans.," *Development*, vol. 125, pp. 3607–3614, 1998.

[27] B. Etemad-Moghadam, S. Guo, and K. Kemphues, "Asymmetrically distributed PAR-3 protein contributes to cell polarity and spindle alignment in early C. elegans embryos," *Cell*, vol. 83, no. 5, pp. 743–752, 1995.

[28] J. L. Watts, B. Etemad-Moghadam, S. Guo, L. Boyd, B. W. Draper, C. C. Mello, J. R. Priess, and K. J. Kemphues, "par-6, a gene involved in the establishment of asymmetry in early C. elegans embryos, mediates the asymmetric localization of PAR-3.," *Development*, vol. 122, no. 10, pp. 3133–3140, 1996.

[29] T.-J. Hung and K. J. Kemphues, "PAR-6 is a conserved PDZ domain-containing protein that colocalizes with PAR-3 in Caenorhabditis elegans embryos," *Development*, vol. 126, no. 1, pp. 127–135, 1999.

[30] J. Rodriguez, F. Peglion, J. Martin, L. Hubatsch, J. Reich, N. Hirani, A. G. Gubieda, J. Roffey, A. R. Fernandes, D. St Johnston, J. Ahringer, and N. W. Goehring, "aPKC cycles between functionally distinct PAR protein assemblies to drive cell polarity," *Dev Cell*, vol. 42, no. 4, pp. 400–415.e9, 2017.

[31] J. Li, H. Kim, D. G. Aceto, J. Hung, S. Aono, and K. J. Kemphues, "Binding to PKC-3, but not to PAR-3 or to a conventional PDZ domain ligand, is required for PAR-6 function in C. elegans," *Dev Biol*, vol. 340, no. 1, pp. 88–98, 2010.

[32] B. Li, H. Kim, M. Beers, and K. Kemphues, "Different domains of C. elegans PAR-3 are required at different times in development," *Developmental Biol.*, vol. 344, no. 2, pp. 745–757, 2010.

[33] L. Boyd, S. Guo, D. Levitan, D. T. Stinchcomb, and K. J. Kemphues, "PAR-2 is asymmetrically distributed and promotes association of P granules and PAR-1 with the cortex in C. elegans embryos.," *Development*, vol. 122, no. 10, pp. 3075–3084, 1996.

[34] W. Driever and C. Nüsslein-Volhard, "A gradient of bicoid protein in Drosophila embryos," *Cell*, vol. 54, pp. 83–93, jul 1988.

[35] F. Tostevin and M. Howard, "Modeling the establishment of PAR protein polarity in the one-cell C. elegans embryo," *Biophys J*, vol. 95, no. 10, pp. 4512–4522, 2008.